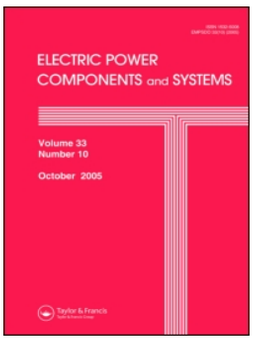

Taylor & Francis
Taylor & Francis Group

Electric Power Components and Systems

ISSN: 1532-5008 (Print) 1532-5016 (Online) Journal homepage: https://www.tandfonline.com/loi/uemp20

Seamless Transfer of Microturbine Generation System Operation Between Grid-connected and Islanding Modes

D. N. Gaonkar , G. N. Pillai & R. N. Patel

To cite this article: D. N. Gaonkar , G. N. Pillai & R. N. Patel (2009) Seamless Transfer of Microturbine Generation System Operation Between Grid-connected and Islanding Modes, Electric Power Components and Systems, 37:2, 174-188, DOI: 10.1080/15325000802388815

To link to this article: https://doi.org/10.1080/15325000802388815

Electric Power Components and Systems, 37:174–188, 2009

ISSN: 1532-5008 print/1532-5016 online
DOI: 10.1080/15325000802388815

Taylor & Francis
Taylor & Francis Group

Seamless Transfer of Microturbine Generation System Operation Between Grid-connected and Islanding Modes

D. N. GAONKAR,[1] G. N. PILLAI,[2] and R. N. PATEL[3]

[1]Department of Electrical Engineering, National Institute of Technology Karnataka, Surathkal, Mangalore (D.K.), Karnataka State, India
[2]Department of Electrical Engineering, Indian Institute of Technology Roorkee, Roorkee, Uttaranchal, India
[3]Department of Electrical and Electronics Engineering, S.S. College of Engineering and Technology, Bilhai

Abstract *The intentional islanding operation of grid-connected distributed generation systems can greatly improve the reliability and quality of the power supply. The existing control techniques for distributed generation systems are designed to operate either in the grid-connected or islanding modes of operation, thus, not allowing for both modes to be implemented and transitioned between. In this article, a novel scheme for automatic mode switching of a microturbine-based distributed generation system between the grid-connected and islanding modes of operation is proposed. The presented scheme is based on the phase angle estimated by the phase-locked loop. The developed phase-locked loop provides an accurate estimation of the phase angle even under unbalanced conditions. The presented scheme does not negatively affect the distributed generation system or utility operations and can work even under matching distributed generation and load power ratings. In this work, back-to-back converters are used to interface the microturbine-based distributed generation system to the grid. Converter control strategies developed for both modes of distributed generation operation is also presented. The simulation results show good accuracy of the proposed scheme.*

Keywords distributed generation, microturbine generation system, grid-connected mode, islanding, islanding detection, phase-locked loop

1. Introduction

The integration of distributed generation (DG) units into the distribution system offers a number of technical, environmental, and economical benefits. In order to achieve these benefits with large penetration of the DG source in an existing utility network, several technical problems must be confronted, such as degradation of system reliability, islanding, power quality problems, and various other safety issues [1]. One of the major concerns in operating DG systems parallel with the grid is the possibility of islanding of DG due to grid disturbances such as network faults. Islanding is a situation in which

Received 8 February 2007; accepted 9 July 2008.
Address correspondence to Prof. D. N. Gaonkar, Department of Electrical Engineering, National Institute of Technology Karnataka, Surathkal, Mangalore (D.K.), Karnataka, 575 025, India. E-mail: dngaonkar@yahoo.co.in

DG installation and a portion of the utility system have become isolated, and the DG continues to operate and serve loads on the circuit [1, 2].

Current practice in design and operation of networks discourage the islanded operation for safety and security reasons [1, 2]. But in recent years, due to a deregulated environment, there is a trend to operate DG in intentional islanding mode in order to meet the uninterrupted, quality electric power demand of the customer. Islanded operation of the DG system during utility outage (intentional islanding) will improve the reliability and helps in maintaining uninterrupted power supply [3, 4]. Therefore, current protection practices of disconnecting the DG units following a disturbance to prevent islanding will no longer be a practical or reliable solution in a deregulated market environment [3]. IEEE Std. 1547-2003 [4] states the need for implementing intentional islanding operation of DG systems.

Existing control techniques for DG systems are designed to operate a system either in the connected or disconnected (islanding) mode to the utility, thus, not allowing for both modes to be implemented and transitioned between them [3]. The dynamic performance of a microturbine generation (MTG) system under various grid disturbance conditions has been studied. In [5], only grid-connected operation of an MTG system was considered. A unified control scheme for operating the DG system both in grid-connected and islanding modes was presented in [6]. A seamless transfer method from grid-connected to islanding mode and vice versa for critical loads was described in [7], where an extra static switch is required. A phase-locked loop (PLL) technique is commonly used in grid-connected converters to provide accurate estimation of phase angle for grid synchronization [8]. A PLL-based flexible transition control strategy for wind energy system with an induction generator is presented in [9]. A PLL structure presented in this work may not give accurate estimation of phase angle during unbalanced grid conditions.

The present trend in DG technology is toward a smaller DG system with a capacity less than 500 kW. An excellent example is a new, fast-growing MTG system. These generation systems are more reliable, have higher operating efficiency, and have ultra low emission levels [10, 11]. They can operate on multi-fuels and are proving to be a supplement to traditional forms of power generation, whether it is stand alone, mobile, remote, or interconnected with the utility applications.

A novel scheme for seamless transfer of MTG system operation between grid-connected and islanding mode and vice versa is proposed in this article. The presented scheme uses the estimated phase angle error obtained by the PLL for islanding detection and re-synchronizing DG to grid. The PLL structure devised in this work can provide accurate estimation of phase angle even under unbalanced grid conditions. A converter control strategy for both grid-connected and islanding modes have been presented. The presented scheme does not negatively affect the DG or utility operations and can work even under matching DG and load power ratings. The performance of the presented scheme is studied through computer simulation.

2. MTG Systems

There are two types of MTG systems that are based on the position of the compressor turbine and generator. The high-speed single-shaft design has a compressor and turbine mounted on the same shaft along with the permanent magnet synchronous generator. The generator generates power at a very high frequency ranging from 1500 to 4000 Hz. The high-frequency voltage is first rectified and then inverted to a normal AC power at 50 or 60 Hz. In another design, the turbine on the first shaft directly drives the compressor,

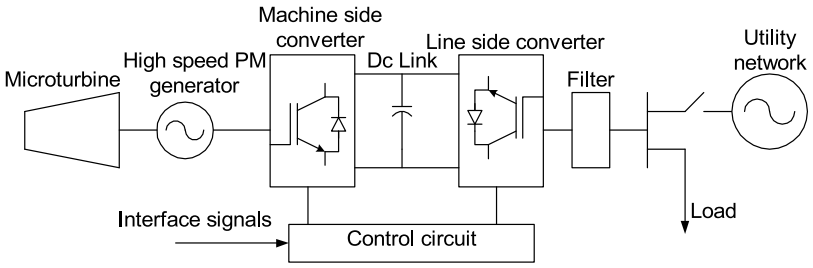

Figure 1. MTG system with back-to-back converter interface.

while a power turbine on the second shaft drives the gearbox and conventional electrical generator (usually induction generator) producing 60-Hz power. The power electronic interface network is a critical component in the single-shaft microturbine design and offers significant challenges. Several topologies exist for interfacing the MTG system to the grid matrix converter [12], cycloconverter [13], and passive inverter and rectifier [11]. Simulation of the electric part of a grid-connected microturbine with back-to-back converter interface was also reported in [14]. The grid-interconnected MTG system using back-to-back converter topology is shown in Figure 1.

The topology shown in Figure 1 allows bidirectional power flow between the converter and the grid, and hence, no separate starting arrangement is required. At the time of starting, the permanent magnet synchronous machine (PMSM) acts as a motor and draws power from the grid to bring the turbine to a certain speed. In this mode, the grid-side converter acts as a controlled rectifier, and the machine-side converter acts as an inverter and provides AC supply to the motor. This is also referred to as the motoring mode operation of the PMSM. During the generating mode, the PMSM acts as a generator and power flows from the MTG system to the grid. The machine-side and grid-side converters act as the controlled rectifier and inverter, respectively. In both modes of operation, the grid-side converter regulates the DC-bus voltage, while the machine-side converter controls the PMSM speed and displacement factor. The Simulink model of the simplified single-shaft microturbine is shown in Figure 2 [15, 16]. This model is based on the gas turbine model presented in [17]. A high-speed permanent magnet synchronous generator model is developed in Simulink using dq-components of the stator voltage and the torque equation in dq-synchronous reference frame [18].

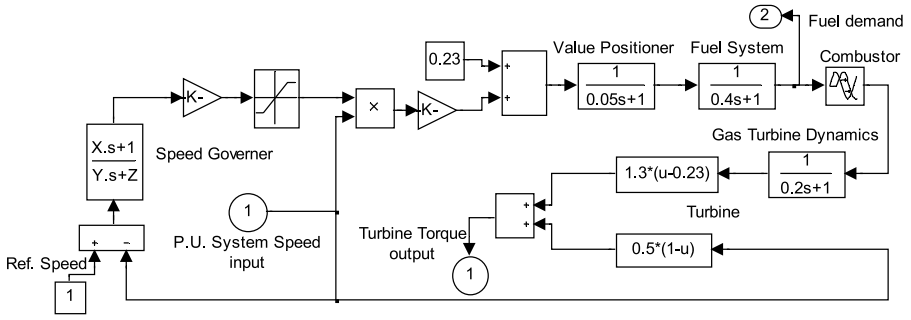

Figure 2. Simulink model of the microturbine.

2.1. Machine-side Converter

Figure 3 shows the Matlab implementation of a two-loop control structure, *i.e.*, the inner and outer control loops in the dq-synchronous reference frame for the drive control system. The commanded speed, ω_{ref}, is pre-calculated according to the turbine output power and set to the optimum speed [19]. Based on the speed error (ew), the commanded q-axis reference current, i_{qref}, is determined through the speed controller. In this system, the following proportional-integral (PI) controller is employed as the speed controller:

$$i_{qref} = K_{P\omega} e_\omega + K_{I\omega} \int e_\omega dt, \tag{1}$$

where $K_{P\omega}$ and $K_{I\omega}$ are the proportional and integral gains of the speed controller, respectively. For higher speed operations of the PMSM, field weakening must be adopted by selecting $i_{dref} < 0$. Based on the current errors, the dq-axis reference voltages are determined by PI controllers as:

$$v_d = K_{Pi} e_d + K_{Ii} \int e_d dt - \omega_r L_q i_q, \tag{2}$$

$$v_q = K_{Pi} e_q + K_{Ii} \int e_q dt + \omega_r (L_d i_d + \lambda_m), \tag{3}$$

where K_{Pi} and K_{Ii} are the proportional and integral gains of the current controllers, respectively. e_d is the d-axis current error ($i_{dref} - i_d$), and e_q is the q-axis current error ($i_{qref} - i_q$). The decoupling terms for the d-axis ($-\omega_r L_q i_q$) and the q-axis ($\omega_r (L_d i_d + \lambda_m)$) are also used in Eqs. (2) and (3), respectively, for the independent control of the d- and q-axis currents. The commanded dq-axis voltages (v_d, v_q) are transformed into a, b, c quantities (v_a, v_b, v_c) and given to the pulse-width modulation (PWM) generator to generate the gate pulse for the machine-side converter.

2.2. Grid-side Converter

Grid-connected Mode. The PQ control strategy with DC-link voltage control is employed for the grid-connected operation of the MTG system. In this scheme, the power injected to the grid is regulated by controlling the injected current. Standard PI controllers are used to regulate the grid current in the dq-synchronous frame in the inner control

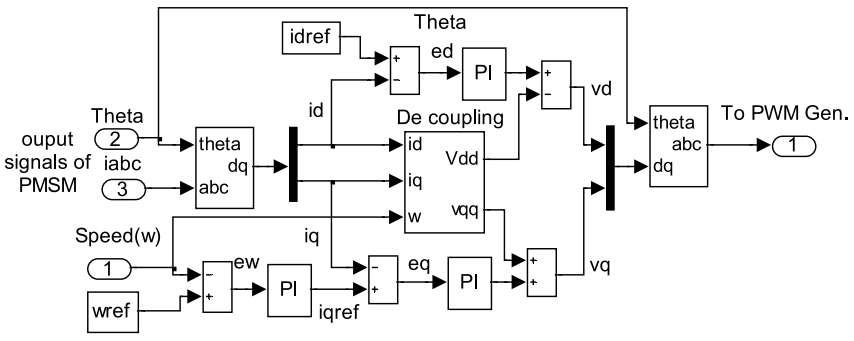

Figure 3. Machine-side converter controller.

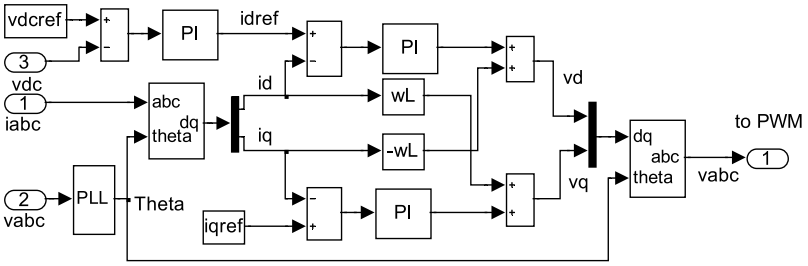

Figure 4. Grid-side converter controller.

loop and the DC voltage in the outer loop. The objective of the supply-side converter is to keep the DC-link voltage constant, regardless of the magnitude and direction of the rotor power. The two-loop control structure for the grid-connected operation is implemented using standard voltage equations in the dq-synchronous reference frame, as given in Eqs. (4) and (5). The inner loop controls the current and outer loop controls the DC-link voltage. The Simulink block diagram of the grid-side converter controller is shown in Figure 4. To have an independent control of the current components, i_d and i_q, the decoupling voltage components are added to the output of PI current controllers:

$$v_d = L_f \frac{di_d}{dt} + R_f i_d - \omega L_f i_q, \tag{4}$$

$$v_q = L_F \frac{di_q}{dt} + R_f i_q + \omega L_f i_d. \tag{5}$$

One of the important requirements in the interconnection design of the power electronic converter interfaced DG system is that of synchronization to the utility system. Synchronism of converter control with the grid is achieved by using a PLL. The Simulink block diagram of the PLL used in this work is shown in Figure 5, where γ is the grid phase angle, and v_x and v_y are the grid voltage components in the stationary reference frame. The philosophy of the PLL is that the sine of the difference between grid phase angle γ and inverter phase angle θ can be reduced to zero using a PI-controller, thus locking the inverter phase to the grid with small arguments ($\sin(\gamma-\theta) \cong (\gamma-\theta) = \Delta\theta$). The output of the PI controller is the inverter output frequency that is integrated to obtain

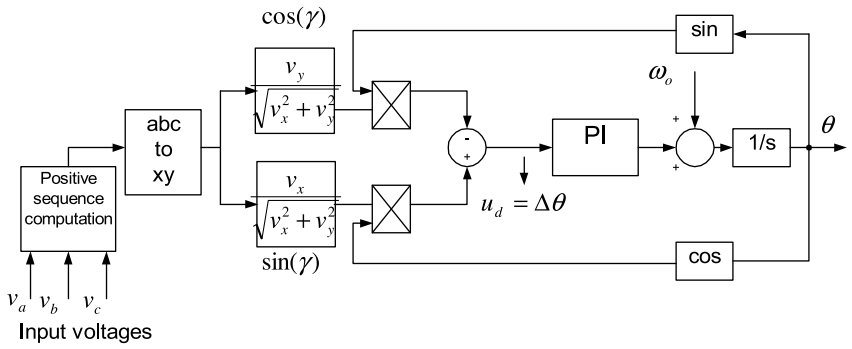

Figure 5. Simulink model of the PLL.

the inverter phase, θ. In order to improve the dynamic response at startup, the nominal frequency of the grid, ω_o is feed-forwarded to the output of the PI-controller.

The major disadvantage of the three-phase PLL is its sensitivity to grid voltage unbalance. Some attempts have been made to extend this method for unbalanced voltages based on the concept of symmetrical components [20]. Here, the positive sequence extraction is represented as given in [20] and is shown in Figure 6. The symmetrical components can be used for signals that are functions of time. Even though the concept is originally defined with respect to phasors, one can extend it to the signals as functions of time.

The idea is to implement complex phasor $a = e^{\pm j120^\circ}$ with an 120° phase shift operator in the time domain. This can be easily implemented in terms of a 90° phase shift operator as $e^{\pm j120^\circ} = -(1/2) \pm (\sqrt{3}/2)e^{j90^\circ}$. Using this, one can derive time domain positive sequence components as given in Eq. (7). The all-pass filter shown in Figure 6 is used to provide a 90° phase shift and is implemented as a first-order filter. The positive sequence extraction unit is based on

$$\begin{bmatrix} v_a^+ \\ v_b^+ \\ v_c^+ \end{bmatrix} = \frac{1}{3}\begin{bmatrix} 1 & a & a^2 \\ a^2 & 1 & a \\ a & a^2 & 1 \end{bmatrix}\begin{bmatrix} v_a \\ v_b \\ v_c \end{bmatrix}, \tag{6}$$

$$v_a^+ = \frac{1}{3}v_a - \frac{1}{6}(v_b + v_c) - \frac{1}{2\sqrt{3}}S_{90}(v_b - v_c), \qquad v_b^+ = -v_a^+ - v_c^+, \quad \text{and} \tag{7}$$

$$v_c^+ = \frac{1}{3}v_c - \frac{1}{6}(v_a + v_b) - \frac{1}{2\sqrt{3}}S_{90}(v_a - v_b). \tag{8}$$

Islanding Mode. The islanding mode operation of a single-shaft MTG system requires a control different from that of the grid-connected mode. In this mode, the system has already been disconnected from the utility; therefore, it no longer regulates the voltage and frequency. Thus, the output voltages are to be controlled in terms of amplitude and frequency, which leads to control of the reactive and active power flow. This is done

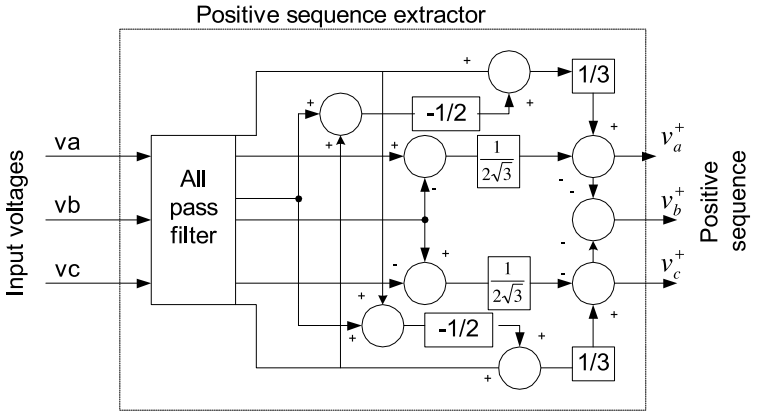

Figure 6. Positive sequence computation unit.

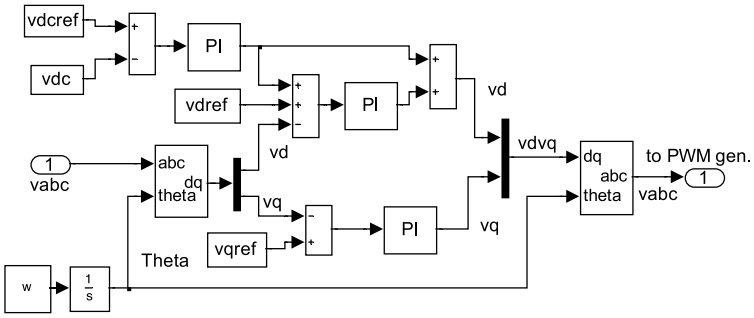

Figure 7. Grid-side converter controller for islanding mode operation.

by controlling the amplitude and frequency of the modulating input signal to the PWM inverter. The control structure for the islanding mode is depicted in Figure 7. It consists of output voltage and DC-link voltage PI controllers. The output controllers control the voltage with a minimal influence from the nature of the load currents or load transients. A standard PI controller operating in a synchronously rotating coordinate system, where v_q is kept to zero, is used. The DC voltage PI controller controls the DC voltage level based on the reference. For a fast response, the output of the DC voltage controller is feed-forwarded to the voltage controller output.

The DC-link voltage controller acts only when the DC-link voltage is below the reference. The voltage reference of the main voltage controller is reduced in order to avoid inverter saturation. The frequency control is done by integrating the constant reference frequency, ω, and using it for coordinate transfer of the voltage components from abc to dq and vice versa.

In islanding mode, when there is more generation than the load demand, the DC-link voltage becomes higher than the reference. In this condition, the damping chopper control is activated, which is shown in Figure 8. The excess energy stored in the DC-link is dissipated in the damping resistor by chopper control and, hence, reduces the DC-link voltage. The control is linear and increases the duty cycle as a function of the over-voltage magnitude. A proportional controller has been implemented, which controls the duty cycle of the switch. In practice, batteries are used to store this excess energy.

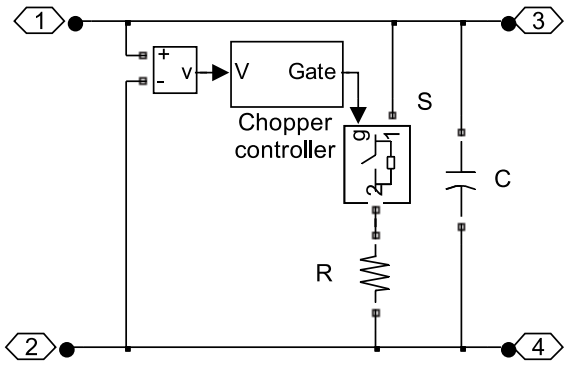

Figure 8. DC-link circuit of MTG system with chopper control.

3. Proposed Seamless Transfer Scheme

The proposed seamless transfer scheme consists of a passive islanding detection and re-closure method. The presented islanding detection method uses the phase angle estimated by the PLL to detect the islanding condition. The re-closure scheme continuously monitors the phase angle and terminal voltage magnitude to determine whether or not the disturbance in the grid is over. This is necessary in order to synchronize the MTG system and to connect back to the grid without any down-time. The PLL block used in inverter control is employed for this scheme; hence, no additional hardware is needed. The structure of the PLL used to determine the phase angle error required by the proposed scheme has been described in Section 2.2.

3.1. Islanding Detection

The algorithm devised for the detection scheme is shown in Figure 9. The algorithm compares the phase angle error ($\Delta\theta$) obtained from the PLL with that of the threshold value. If $\Delta\theta$ exceeds the set threshold limit, then islanding is confirmed. At the same time, control of the inverter is transferred from the current control mode (grid-connected) to the voltage-control mode (islanding mode). During the grid-connected mode, $\Delta\theta$ is approximately zero. Once the grid fails, the phase angle error starts to increase. The $\Delta\theta$ value is obtained by the PLL as explained in Section 2.2. This algorithm gives accurate results even under matching load conditions.

3.2. Re-closure Method

The re-closure algorithm for connecting the MTG system to the grid, when the utility recovers from the disturbance, is shown in Figure 10. The two main obstacles in re-synchronizing the DG system to the grid are matching voltage magnitude and phase angle between the converter and the grid. If this is not done, a large transient will take place that will damage the MTG system. The re-closure algorithm continuously monitors the terminal voltage of the grid and MTG system. Both voltage magnitudes are compared. As per IEEE Std. 1547-2003 [4], the DG terminal voltage should be between 1.1 and 0.88 p.u. of the nominal voltage. Both voltages should be approximately equal to avoid large transients during re-connection to grid. Once the voltages are approximately equal,

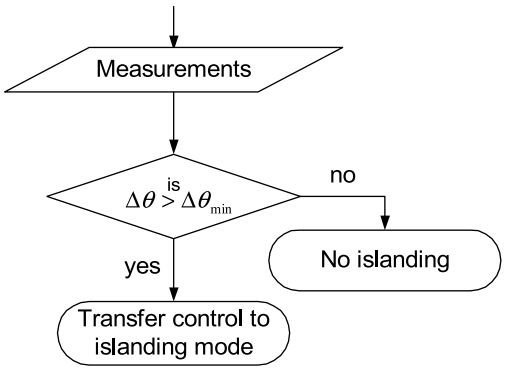

Figure 9. Islanding-detection scheme.

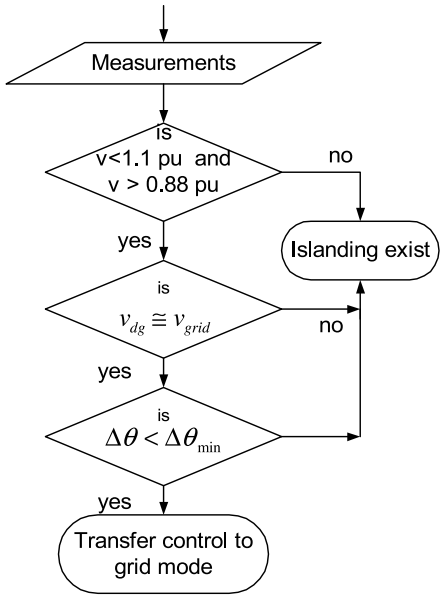

Figure 10. Re-closure scheme.

then the algorithm compares the $\Delta\theta$ value obtained from the PLL with the set threshold limit. As long as these minimum requirements are met (voltage and phase angle), there are no major issues in reconnection of islanded systems to the utility. This avoids the de-energizing of the system and down-times.

4. Results and Discussion

Figure 11 shows the simulation model implemented in SimPowerSystems of MATLAB to study the performance of the MTG system operation in grid-connected and islanding modes. The utility network is represented by a three-phase sinusoidal source with its

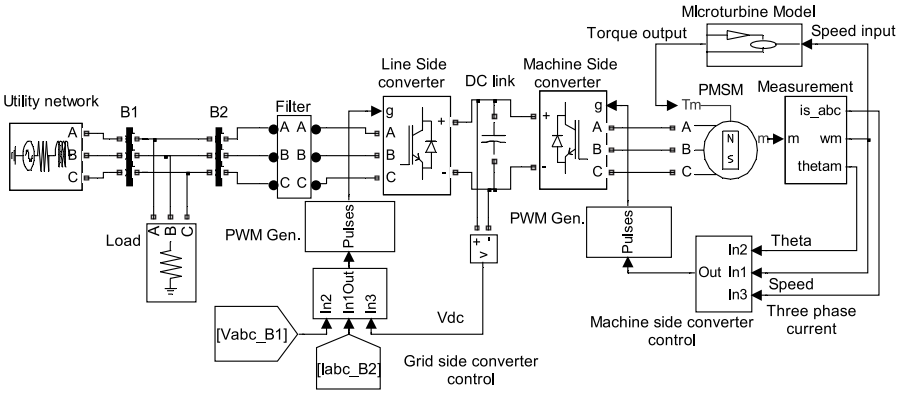

Figure 11. Matlab/SimPowerSystems implementation of MTG system connected to grid.

Table 1
Simulation parameters for the model shown in Figure 11

Grid parameters	480 V, 60 Hz, $R_s = 0.4\ \Omega$ and $L_s = 2$ mH
Filter parameters	$L = 0.97$ mH, $R = 0.21\ \Omega$
Switching frequency	Grid side converter = 8 KHz Machine side converter = 20 KHz
DC-link capacitance	5000 μF
PI controllers sampling time	100 μsec
PMSM parameters	480 V, 30 kW, 1.6 KHz, 96,000 rpm $R_s = 0.25\ \Omega$, $L_q = L_d = 0.0006875$ H
Microturbine parameters	Gain(K) = 25, $X = 0.4$, $Y = 0.05$, and $Z = 1$

impedance. A series resistor and inductor (RL) filter is used at the grid side of the MTG system. The simulation parameters of the model are given in Table 1.

The MTG system takes p.u. speed of the PMSM as input. The torque output of the microturbine is given as an input mechanical torque (T_m) to the PMSM. The direction of torque T_m is positive during the motoring mode and made negative during the generating mode of the PMSM. The machine side converter controller takes the rotor angle speed and three-phase stator current signals of the PMSM as inputs. In all presented cases, the voltage across the capacitor is zero at the starting of simulation.

4.1. Utility Interactive to Islanding Mode

The MTG system acts as a motor during starting to launch the microturbine. Once the microturbine reaches the speed of 3142 rad/sec at $t = 0.4$ sec, the PMSM is operated as a generator by changing the direction of its input torque to negative. During generating mode power flows from the MTG system to the grid, the phase angle error between the grid voltage and converter voltage is approximately zero, as shown in Figure 12(a). In the grid-connected mode, the MTG system is operated to inject 28 kW, as shown in Figure 12(b). The other parameter variations during this mode of operation are given in Figures 12 and 13.

At $t = 1.4$ sec, utility connection to the DG is disconnected by opening the circuit breaker. This results in the formation of a planned islanding situation comprising the local load and MTG system. Opening of the circuit breaker can occur due to the faults and other grid disturbances. When the circuit breaker is opened, the phase angle difference ($\Delta\theta$) between grid voltage and inverter voltage obtained from the PLL starts to increase. The islanding detection algorithm given in Figure 9 continuously monitors the $\Delta\theta$ variation. Once $\Delta\theta$ crosses the threshold limit of 0.08 rad, then islanding is detected and converter control switches to the islanding mode. The algorithms detect the islanding condition and transfer the control almost instantaneously. The variation of $\Delta\theta$, active power, reactive power, and the i_d component of the injected grid current are shown, respectively, in Figures 12(a), 12(b), 12(c), and 12(d). During this transition, a dip in DC-link voltage can be observed from Figure 12(e). This is due to the variation in active power output of the MTG system. During the islanding mode, the MTG system supplies the power requirement of the load. Hence, current supplied by the utility is zero, as observed from Figure 13(a).

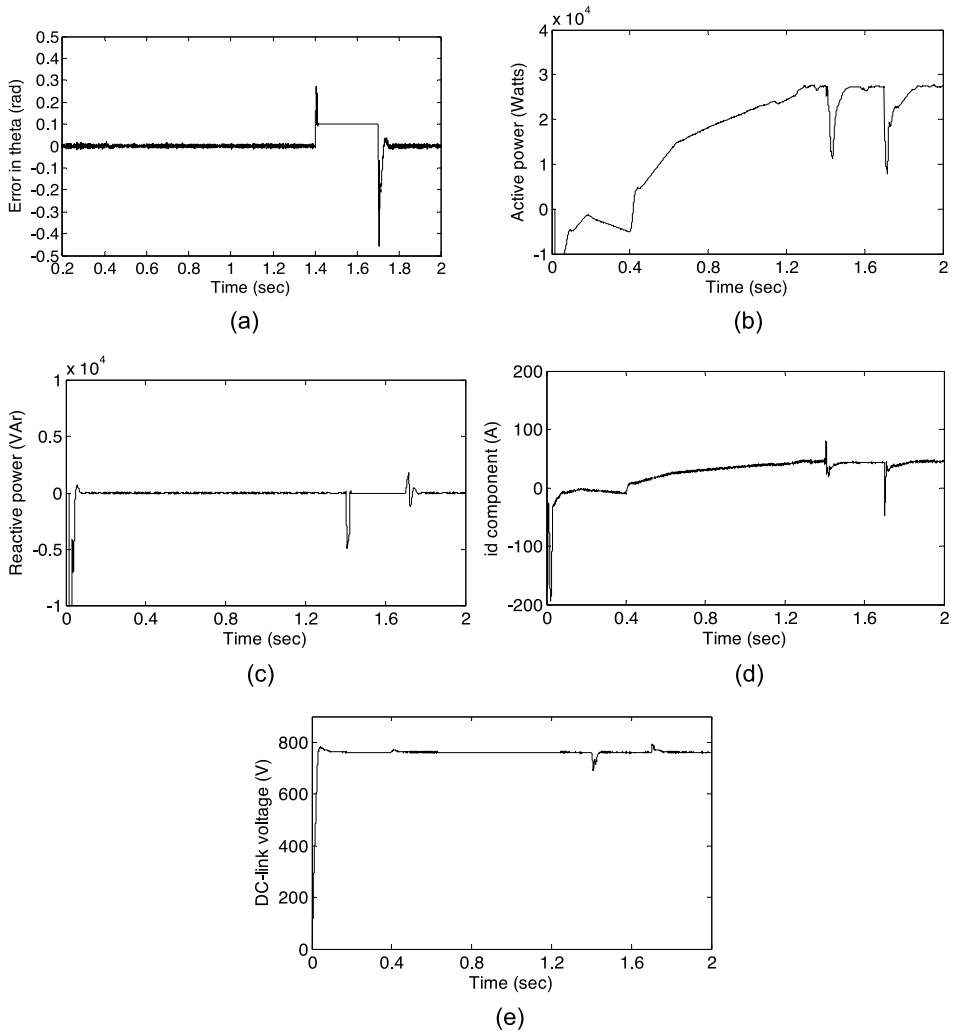

Figure 12. (a) Phase angle error ($\Delta\theta$) variation, (b) active power injected to the grid by MTG system, (c) reactive power exchanged with the grid, (d) i_d component of the injected grid current, and (e) DC-link voltage.

4.2. Islanding to Utility Interactive Mode

At $t = 1.7$ sec, the synchronization process starts to reconnect the DG to utility. The re-closure algorithm compares the grid voltage magnitude and phase angle with the MTG system's terminal voltage and phase angle. When the utility voltage magnitude approximately matches that of the MTG system, and $\Delta\theta$ is less than the threshold, then DG is connected to the utility. The variation of $\Delta\theta$, active power, reactive power, and the i_d component of the injected grid current and the DC-link voltage during this transition are shown, respectively, in Figures 12(a), 12(b), 12(c), 12(d), and 12(e).

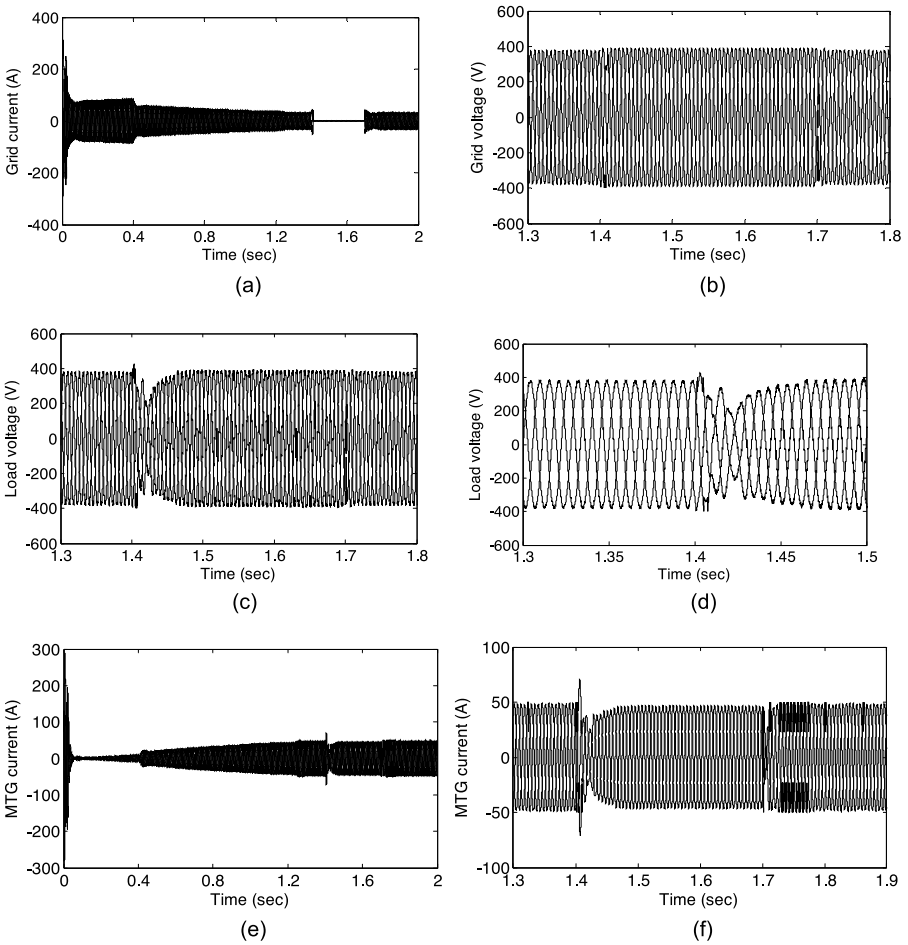

Figure 13. (a) Line current of the grid, (b) phase voltage of the grid, (c) phase voltage of the load, (d) detailed variation of load phase voltage, (e) line current at the grid side of MTG system, and (f) detailed variation of line current at the grid side of MTG system.

4.3. Load Switching

The load-switching case has been considered to check whether the algorithm can differentiate load-switching and islanding conditions. In the grid-connected mode of operation of the MTG system at $t = 1.6$ sec, the load is increased from the initial value of 36 kW to 50 kW. This can be observed from the variation in the line current of the load, as shown in Figure 14(a). At the point of switching, a small increase in the phase angle error ($\Delta\theta$) obtained from the PLL from its normal variation can be seen in Figure 14(b). The change in the error ($\Delta\theta$) due to the load switching is very small compared to the threshold limit of 0.08 rad. Hence, the detection scheme did not consider it as an islanding case. Thus, there is no switching of converter control from the current-controlled mode to voltage-control mode.

During the islanding mode of the MTG system, if the load demand is less than the rated output of the MTG system, then the DC-link voltage increases. The increased

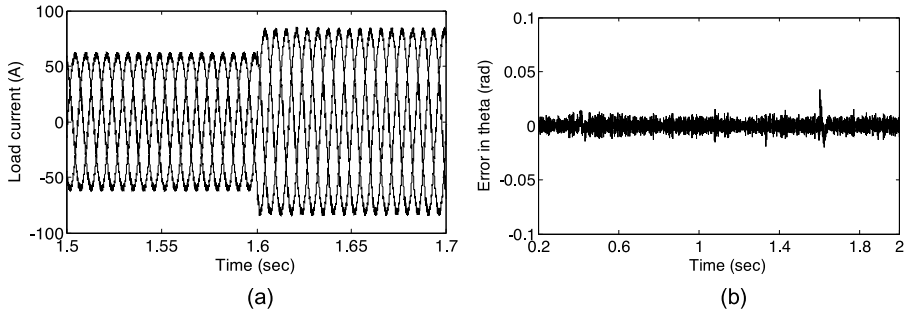

Figure 14. (a) Variation of the load current and (b) variation in the phase angle error ($\Delta\theta$) during load change.

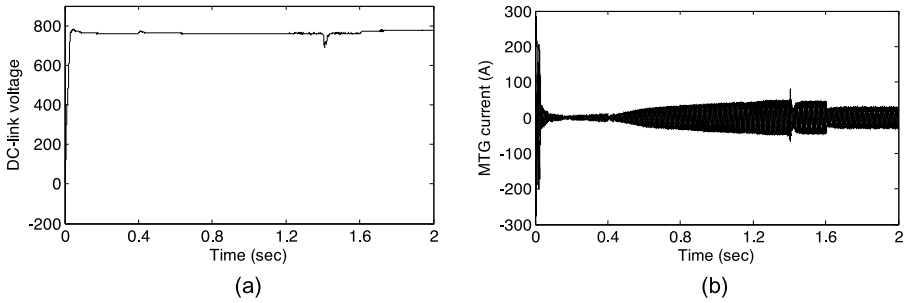

Figure 15. (a) DC-link voltage and (b) variation in the current at the grid side of the MTG system.

energy should be stored in a battery or dissipated in a resistor using chopper control in order to regulate the DC-link voltage to 760 V. The chopper control circuit used in this work is shown in Figure 8. To analyze this condition, a case has been considered. In this study, the MTG system is islanded due to the opening of a circuit breaker at $t = 1.4$ sec. At the point of islanding, a dip in the DC-link voltage can be observed from the Figure 15(a). When the DC-link voltage is below 760 V, the DC-link voltage controller will regulate it to its normal value. At $t = 1.6$ sec, the load is decreased from 28 kW to 14 kW. This can be observed from the variation in the injected current by the MTG system, as shown in Figure 15(b). The increased energy in the DC-link is dissipated in the damping resistor (R). This is done by controlling the on and off time of the switch at a very high frequency in order to regulate the DC-link voltage to 760 V. This can be observed from Figure 15(a).

5. Conclusions

A seamless transfer scheme for MTG system operation between grid-connected and intentional islanding mode is proposed in this article. It is seen that the presented scheme can successfully switch the operation of the MTG system between utility interactive and islanding modes without any detrimental transients. The result presented also shows that the proposed islanding-detection technique can successfully differentiate between load-switching and islanding conditions. The presented automatic mode switching scheme helps in providing continuous power supply to the customer even during outages of the

utility. The presented islanding detection algorithm has proved to be efficient and can detect islanding even during matching load and DG capacity conditions. Also, it has been seen that the scheme does not operate for load switching. The scheme is simple and can be implemented without any additional hardware. The simulation results show that the converter control strategy developed is capable of maintaining both voltage and frequency within the standard permissible levels during islanded operation of the MTG system.

References

1. Barker, P. P., and De Mello, R. W., "Determining the impact of distributed generation on power systems: Part 1—Radial distribution systems," *Proc. IEEE Power Eng. Soc. Summer Mtg.*, Vol. 3, pp. 1645–1656, 2000.
2. Villeneuve, P. L., "Concern generated by islanding," *IEEE Power Energy Mag.*, Vol. 2, No. 3, pp. 49–53, 2004.
3. Barsali, S., Ceraolo, M., Pelacchi, P., and Poli, D., "Control techniques of dispersed generators to improve the continuity of electricity supply," *Proceedings of the IEEE PES Winter Meeting*, Vol. 2, pp. 27–31, 2002.
4. IEEE, "IEEE standard for interconnecting distributed resources with electric power systems," IEEE Std. 1547-2003, 2003.
5. Gaonkar, D. N., Pillai, G. N., and Patel, R. N., "Dynamic performance of microturbine generation system connected to grid," *J. Elect. Power Compon. Syst.*, Vol. 36, No. 10, pp. 1031–1047, 2008.
6. Illinda, M., and Venkatramanan, G., "Control of distributed generation systems to mitigate load and line imbalances," *Proceedings of the IEEE Electronics and Specialists Conference*, Vol. 4, pp. 2013–2201, 2002.
7. Tirumala, R., Mohan, N., and Henze, C., "Seamless transfer of grid-connected PWM inverters between utility-interactive and stand-alone modes," *Proc. 17th Ann. IEEE Appl. Power Electron. Conf. Exposit.*, Vol. 2, pp. 1081–1086, 2002.
8. Chung, S.-K., "Phase-locked loop for grid-connected three-phase power conversion systems," *Proc. Inst. Elect. Eng.*, Vol. 147, No. 3, pp. 213–219, 2000.
9. Teodorescu, R., and Blaabjerg, F., "Flexible control of small wind turbines with grid failure detection operating in stand-alone and grid-connected mode," *IEEE Trans. Power Electron.*, Vol. 19, No. 5, pp. 1323–1332, 2004.
10. Scott, W. G., "Microturbine generators for distribution systems," *IEEE Industry Appl. Mag.*, Vol. 4, No. 3, pp. 57–62, 1998.
11. Al-Hinai, A., and Feliachi, A., "Dynamic model of microturbine used as a distributed generator," *Proceedings of the 34th South Eastern Symposium on System Theory*, Huntsville, AL, pp. 209–213, 18–19 March 2002.
12. Nikkhajoei, H., and Iravani, R., "A matrix converter based microturbine distributed generation system," *IEEE Trans. Power Delivery*, Vol. 20, No. 3, pp. 2182–2192, 2005.
13. Azmy, A. M., and Erlich, I., "Dynamic simulation of fuel cells and microturbines integrated with a multi-machine network," *Proceedings of the IEEE Bologna Power Tech Conference*, Vol. 2, pp. 2212–2219, Bologna, Italy, 2003.
14. Fethi, O., Dessaint, L. A., and Al-Haddad, K., "Modeling and simulation of the electric part of a grid connected micro turbine," *Proceedings of the IEEE PES General Meeting*, Vol. 2, pp. 2212–2219, 2004.
15. Hajagos, L. M., and Berube, G. R., "Utility experience with gas turbine testing and modelling," *Proc. IEEE PES Winter Mtg.*, Vol. 2, pp. 671–677, 2001.
16. Gaonkar, D. N., and Patel, R. N., "Modeling and simulation of microturbine based distributed generation system," *Proceedings of the IEEE Power India Conference*, New Delhi, India, pp. 256–260, 10–12 April 2006.

17. Rowen, W. I., "Simplified mathematical representations of heavy duty gas turbines," *ASME Trans. J. Eng. Power*, Vol. 105, No. 4, pp. 865–869, 1983.
18. Pillai, P., and Krishnan, R., "Modeling, simulation, and analysis of permanent-magnet motor drives, Part I: The permanent-magnet synchronous motor drive," *IEEE Trans. Indl. Appl.*, Vol. 25, No. 2, pp. 265–273, 1989.
19. Morimoto, S., Sanada, M., and Takeda, Y., "Wide speed operation of interior permanent magnet synchronous motors with high performance current regulator," *IEEE Trans. Indl. Appl.*, Vol. 30, pp. 920–926, 1994.
20. Ghartemani, M. K., and Iravani, M. R., "A method for synchronization of power electronic converters in polluted and variable frequency environment," *IEEE Trans. Power Syst.*, Vol. 19, No. 3, pp. 1263–1270, 2004.